Progress in Organic Coatings 170 (2022) 107009

Contents lists available at ScienceDirect

Progress in Organic Coatings

journal homepage: www.elsevier.com/locate/porgcoat

Superhydrophobic PDMS coated 304 stainless-steel mesh for the removal of HDPE microplastics

O. Rius-Ayra *, A. Biserova-Tahchieva, V. Sansa-López, N. Llorca-Isern

CPCM Departament de Ciència dels Materials i Química Física, Facultat de Química, Universitat de Barcelona, Martí i Franquès 1 - 11, 08028 Barcelona, Spain

ARTICLE INFO

Keywords:
Superhydrophobic
Superoleophilic
Microplastics
Oil/water separation
PDMS

ABSTRACT

The use of microplastics is a global issue that affects the environment, the economy and human health. Here we describe a superhydrophobic 304 stainless steel obtained by combining chemical etching and PDMS modification. Among other techniques, field emission scanning electron microscopy (FE-SEM) and high-resolution X-ray photoelectron spectroscopy (HR-XPS) were used to identify the hierarchical structure as well as the chemical composition of the surface. The stainless-steel mesh was superhydrophobic (159°) and superoleophilic (0°). The coating presented high stability against abrasion of SiC abrasive paper as well as in the presence of different pH values in acidic or alkaline conditions. In addition, taking advantage of the coating's wetting properties, we show that the superhydrophobic surface can also be used to remove high-density polyethylene microplastics from water. A surface mechanism promoting the removal or microplastics is also proposed, considering the surface properties of the solid pollutants as well as the wetting properties of the superhydrophobic coating.

1. Introduction

Today, solid pollutants represent a major issue all over the world, exerting a major impact on the economy, the environment and human health. Specifically, solid pollutants like microplastics (MP) are emerging pollutants that are found worldwide [1–3].

Several methods are available for separating MP from water, such as air flotation, electrooxidation or sand filtration. However, they are <99 % efficient and require other techniques to achieve complete removal of MP [4,5]. Various technologies have been used to explore innovative ways to capture and remove MP from water. The use of $BiVO_4$ and Fe_3O, combining photocatalytic and magnetic properties, allowed self-propelled robots to degrade MP such as polylactic acid and polycaprolactone [6]. Magnetite nanoparticles have also been used to generate a stable twister-like structure under a magnetic field, since a colloid layer on the water–air interface provided a magneto movable system that allowed the removal of microplastics from the air-water interface [7]. In another study an assembled layered double oxide made of three-dimensional graphene-like carbon was also used to remove polystyrene, and the removal mechanism was identified on the basis of the differences in interaction between the material and the microplastics [8].

In this scenario it is necessary to provide alternatives with extremely high efficiencies that ensure complete removal of microplastics, by taking into account the phases that surround them: namely, water and air. As a result, superhydrophobic materials play a key role in the removal of pollutants from water. Superhydrophobicity is defined by the water contact angle (WCA) > 150°, a sliding angle (SA) and a contact angle hysteresis (CAH) lower than 10° [9,10]. Additionally, in order to achieve extremely high contact angles, the surface of materials has to be modified to obtain a hierarchical structure, combining micro and nano structures, with chemical compounds that tend to reduce the surface free energy and change the wetting properties from hydrophilicity to superhydrophobicity [11–13]. Among all these compounds, polydimethylsiloxane (PDMS) is particularly promising because it is completely sustainable, chemically inert, and has good thermal stability and low surface free energy (19.8 mN/m at 20 °C) [14–17]. Moreover, because of its chemical formula $(CH_3[Si(CH_3)_2O]_nSi(CH_3)_3)$ where n = number of monomers, PDMS presents different molecular interactions between silicone and MP such as oleophilic interactions to the water–oil interface [18,19] or hydrogen bond interactions, van der Waals forces, electrostatic interactions and σ-p and p-p conjugations [20]. For this reason, superhydrophobic surfaces are promising materials for the removal of different kinds of pollutants such including immiscible solvents like oils with low oil contact angles (OCA) [21–23], miscible solvents such as ethanol [24,25] or even dyes [26–28]. Specifically, meshes

* Corresponding author.
E-mail address: oriolriusayra@ub.edu (O. Rius-Ayra).

https://doi.org/10.1016/j.porgcoat.2022.107009
Received 11 March 2022; Received in revised form 19 May 2022; Accepted 26 June 2022
Available online 5 July 2022

and membranes have been used to separate oil from water [29–31]. However, the use of stainless steel (SS) has not been extensively investigated; in the few studies available the type of SS is not reported [32–36]. Therefore, despite the fact that meshes allow the removal of oils, the separation of solid pollutants such as MP by using superwettable materials is still in its infancy.

Here we describe a superhydrophobic 304 stainless steel mesh coated with PDMS (PDMS@304SS) that is effective in removing HDPE microplastics from water, taking advantage of its wetting properties. First the 304 SS mesh was etched to achieve the necessary hierarchical structure, and then it was coated with PDMS to reduce the surface free energy of the system and to confer superhydrophobicity with a WCA = 159 ± 5° and superoleophilicity OCA = 0 ± 1°. Additionally, the coated surface removed HDPE-MP with an efficiency of 99 ± 1 % without leaving solid pollutants in water. Moreover, the removal process was attributed to the wetting properties of the microplastics and the PDMS@304SS as well as the interparticle interactions in water and oil.

2. Experimental procedure

2.1. Superhydrophobic mesh

An AISI 304 stainless-steel mesh (304 SS) with the following composition (%): C ≤ 0.08, Si ≤ 1.00, Mn ≤ 2.00, $P \leq 0.045$, S ≤ 0.030, 18.0 ≤ Cr ≤ 20.0, 8.0 ≤ Ni ≤ 11.0, a hole size of 0.4 mm^2 and 0.2 mm of filament diameter was used as a substrate 2 × 2 cm^2 in size (Fig. S1). The experimental procedure involved four steps for conferring superhydrophobic properties to the mesh (Fig. 1). The substrates were ground with SiC P180 abrasive paper and rinsed in deionized water (DI) and then in ethanol to remove the impurities. After this, the substrates were etched using a 2 M $FeCl_3$ in DI water, HCl 37 % (*w*/w) and H_2O_2 5 % (w/w) in 15:1:1 proportion solution (all reactants purchased from Scharlau) for 10 min at room temperature. Next, the mesh was cleaned with DI water and dried in the oven at 60 °C for 1 h. Then, the oxidized substrates were immersed in a 1 % *w*/w PDMS (purchased from Sylgard 184 Silicone Elastomer) solution in THF (purchased from Riedel-de Haël) for 30 min at room temperature. After this, the samples were dried and cured at 55 °C in the oven for 20 h.

2.2. Durability tests

The durability of the superhydrophobic PDMS@304SS mesh was evaluated by two methods: first, by keeping in contact aqueous solution droplets at different pH values in acid or alkali solution (pH = 0, 1, 4, 7, 9, 12 and 14) using HNO_3, CH_3COOH, H_2O, NH_3 and NaOH respectively with the mesh surface for 10 min; and second, by means of an abrasive grinding paper test in order to study the durability under severe abrasive conditions. The superhydrophobic PDMS@304SS mesh was placed in contact with SiC P1200 grinding paper and was moved 20 cm across, while a constant load of 5 kPa was applied. After each cycle, the surface was cleaned with forced air and then both the WCA and the SA were measured three times at the same place where the abrasion was performed.

2.3. Microplastics removal

High density polyethylene (HDPE) MP (purchased from Abifor) with a size = 133 ± 34 μm were used for removal from a 3.5 % *w*/w NaCl aqueous solution (pH = 7.00). Then, 30 mL of the aqueous solution was prepared for the further addition of 20 mg of MP. After this, 5 mL hexane (coloured with Red O biological stain, both purchased from Scharlab) were added to the mixture and stirred. The separation was carried out in a lab-made system that consisted of a dropping funnel in which the solution containing both phases (organic and aqueous) was poured at 3.0 mL/s (the stopcock was completely opened), 1.5 mL/s and 1.0 mL/s (the stopcock was partially open and let the MP pass through it); an inverted Claisen adapter where the superhydrophobic PDMS@304SS mesh was located with a tilt of 1° corresponding to a sliding angle and two beakers to collect the two separated phases. After this, the mesh was dried in the fume hood (55 °C) to further weigh the retained MP mass and the collected mass of HDPE-MP in the beaker. This procedure was repeated three times washing the superhydrophobic substrate with ethanol after

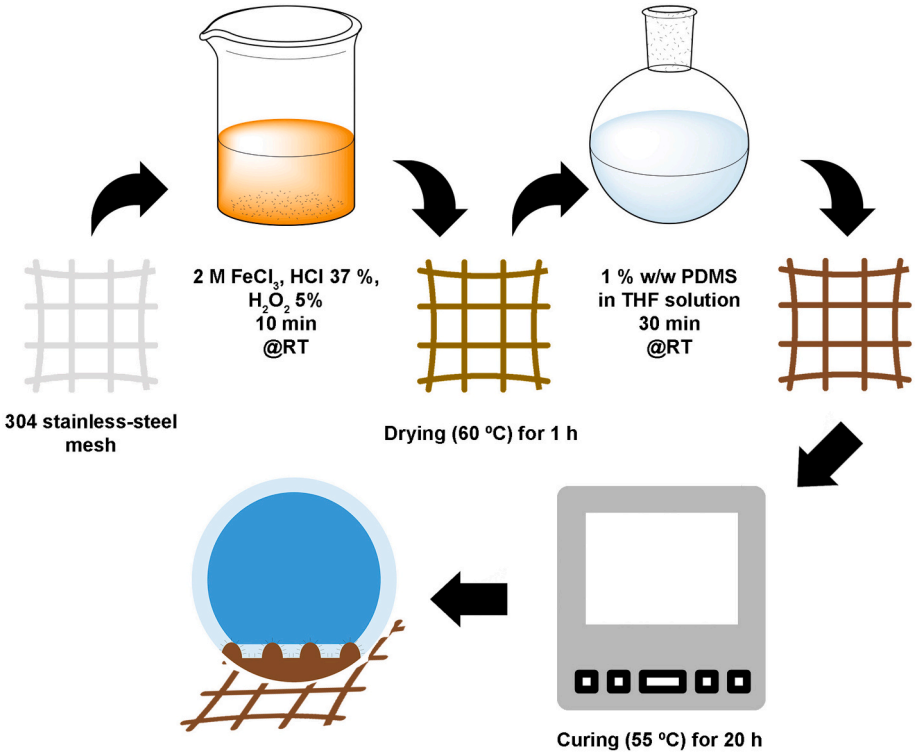

Fig. 1. Experimental procedure for obtaining the superhydrophobic PDMS@304SS mesh for the removal of HDPE-MP.

each test. A reusability test was also carried out to determine how the removal process would affect the wetting properties of the superhydrophobic surface. The method described was repeated several times and after each reuse, the surface was cleaned with absolute ethanol until there was no evidence of any remaining oil or HDPE-MP. Finally, the process was repeated.

3. Characterization techniques

In order to fully understand the role of reactants and the morphology obtained, several characterization techniques were used to determine the structure and the chemical composition. The surface of the superhydrophobic PDMS@304SS mesh was characterized on a JEOL J-7100 field emission scanning electron microscope (FESEM) in order to study its detailed morphology, while EDS microanalysis was used to determine the semiquantitative elemental composition in three different positions of each sample. The roughness (RMS, root mean square) was determined on the surface with the Leica DCM3D confocal microscope, using a white beam as the light source. To establish the chemical composition of the coating obtained, infra-red spectroscopy was also used to determine the presence of PDMS; for this purpose, Attenuated Total Reflectance Fourier Transform Infrared Spectroscopy (ATR-FTIR) was used in the range 4000–525 cm^{-1} at a resolution of 4 cm^{-1} with an instrument (Fourier Bomem ABB FTLA). Additionally, High-Resolution X-Ray Photoelectron Spectroscopy (HR-XPS) was used on a PHI ESCA-5500 using a monochromatic X-ray source (Kα(Al) = 1486.6 eV and 350 W) and Multipak (9.8) was used for the deconvolution analysis. The wetting properties were also carefully studied by determining the static water contact angle (WCA), contact angle hysteresis (CAH) and sliding angle (SA) using the sessile method involving a Levenhuk digital microscope and 3.5 μL of DI water at room temperature. The same method was used to measure the oil contact angle (OCA) with hexane (purchased from Panreac). In the case of HDPE-MP the contact angle measurements were performed as follows: microplastics were sprinkled over a glass slide containing an adhesive before being flattened by another glass slide to prevent roughness effects, and the excess powder was removed. The ImageJ software was used to measure water and oil contact angles. The reported values are the average of three measurements of droplets at different parts on the surface.

4. Results and discussion

4.1. Surface characterization

The FESEM microscope analysis was used to show the semi-quantitative elemental composition as well as the surface morphology throughout the process (Fig. 2): before the surface modification (first column), after the chemical etching (second column) and followed by PDMS coating (third column). As can be seen in the first row (Fig. 2 a–c) and their magnification (Fig. 2 d–f) the unmodified mesh (Fig. 2 a and d) was smooth and did not present any kind of cavity or roughness. Additionally, the EDS (Fig. S2) as well as the EDS mapping (Figs. 2 g and S2) present the main elements of the alloy (Fe and Cr) and a low Si peak that was assigned as minor element of the 304 SS. After chemical etching

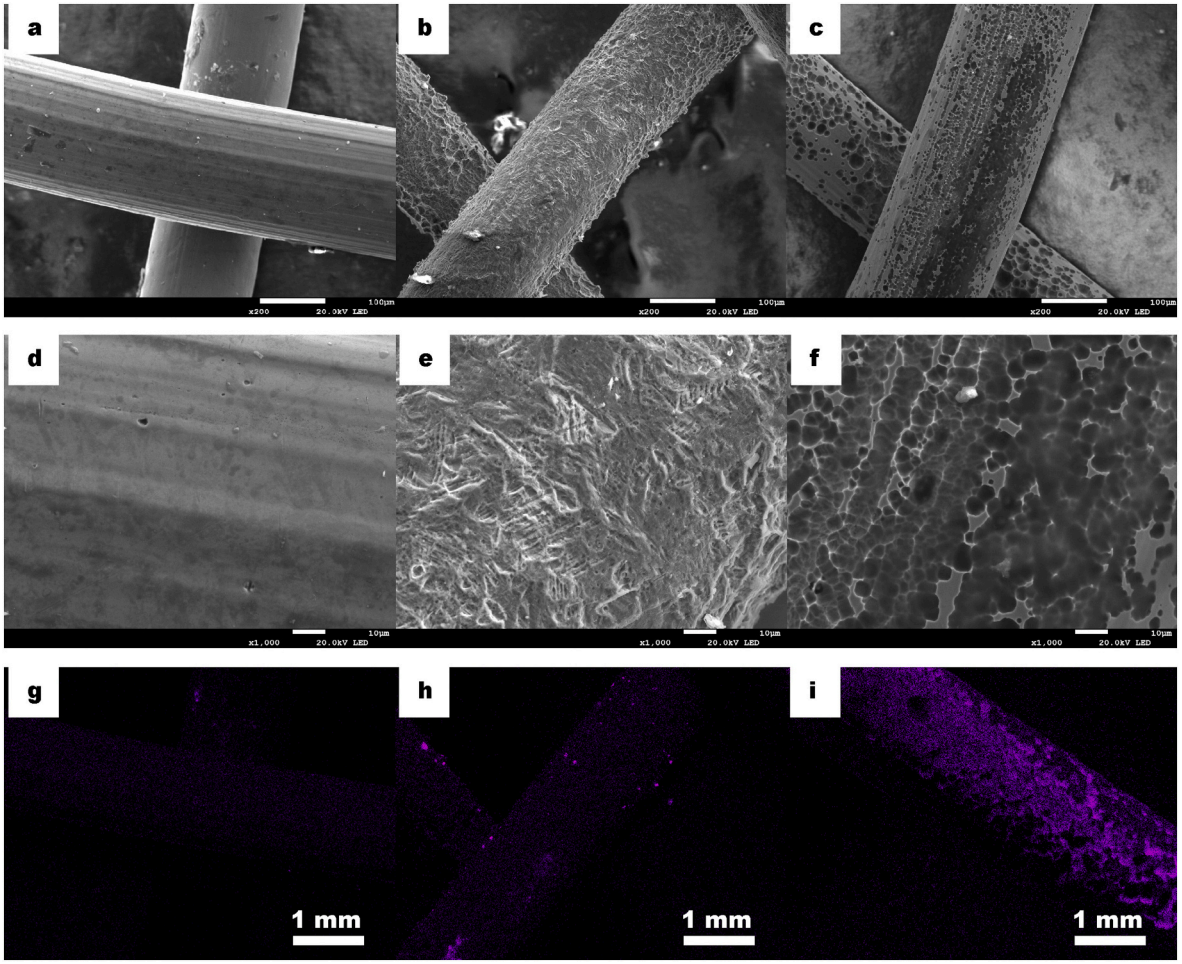

Fig. 2. FESEM micrographs of the 304 SS mesh during the surface modification process: a) unmodified 304 SS mesh, b) after chemical etching, and c) coated with PDMS; d–f) are respectively their magnifications, and g–i) EDS compositional maps after each step as described previously.

the 304 SS surface morphology changed abruptly and showed cavities throughout the surface (Fig. 2 b and e) and the presence of Si increased slightly (Fig. 2 h), indicating that the surface was etched as it also showed an increase in O signal in the EDS and its map (Fig. S3). Once the surface was coated with PDMS (Fig. 2 c and f) the morphology of the cavities changed with dif6pferent sizes at the microscale, and these cavities presented themselves to different nanocavities, leading to the well-known hierarchical structure necessary to confer superhydrophobic properties. Additionally, the EDS map (Fig. 2 i) showed an increase in Si signal that was also showed in the EDS (Fig. S4) and also an increase in C and O in its corresponding EDS map (Fig. S4). The roughness (RMS) of the mesh was also measured after each step. Initially, it was smooth (RMS = 0.52 ± 0.1 μm) while after chemical etching it increased up to 1.62 ± 0.5 μm, indicating that the surface was clearly etched and several cavities were formed, in agreement with the FESEM micrographs. Finally, once the surface was coated with PDMS the RMS also increased to 2.54 ± 0.1 μm, generating larger cavities formed by the combined roughness achieved after chemical etching and PDMS coating.

These results clearly show that the surface of the 304 SS mesh was completely coated with PDMS; after coating the etched surface, the presence of silicon, carbon and oxygen, as main elements of PDMS, increased. These results can be attributed to the fact that after chemical etching the oxidized surface presents hydroxyl groups (—OH) at the surface level, which improves the interaction with the used solution (PDMS in THF) and promotes the formation of a PDMS coating layer at the surface level of the 304 SS mesh [37]. In order to measure the PDMS coating thickness, the size of the filament mesh was measured at three different positions before the surface modification treatment (179 ± 5 μm), after the chemical etching (150 ± 6 μm), and finally after PDMS surface modification (155 ± 3 μm). These results show that the 304 SS mesh was firstly etched, and its diameter decreased, but that after the PDMS modification it increased slightly, obtaining a PDMS thickness of 2.5 ± 9 μm. FESEM micrographs showed that the 304 SS mesh surface was notably etched, while the EDS revealed the constituents of the mesh as well as the presence of oxygen and silicon from PDMS. The chemical etching caused the formation of an oxidized layer corresponding to the micro and nanocavities observed, leading to a hierarchical structure which, combined with the presence of PDMS coating, reduces the surface free energy and confers superhydrophobicity on the modified mesh.

4.2. Chemical characterization

In order to determine the presence of PDMS at the surface level of the mesh obtained, ATR-FTIR and HR-XPS techniques were used to establish the chemical composition of the samples. Fig. 3 a corresponds to the ATR-FTIR PDMS coated mesh with PDMS and shows a wide band between 3700 cm^{-1} and 3100 cm^{-1} corresponding to vO-H of the oxide layer and ca. 3000 cm^{-1} the band assigned to $v_{as}CH_3$. Between 1600 cm^{-1} and 1700 cm^{-1} there was a weak band attributed to δO—H [38]. A very intense peak ca. 1100 cm^{-1} was assigned to vSi—O while bands found ca. 1250 cm^{-1} and ca. 800 cm^{-1} were assigned to δSi—C and

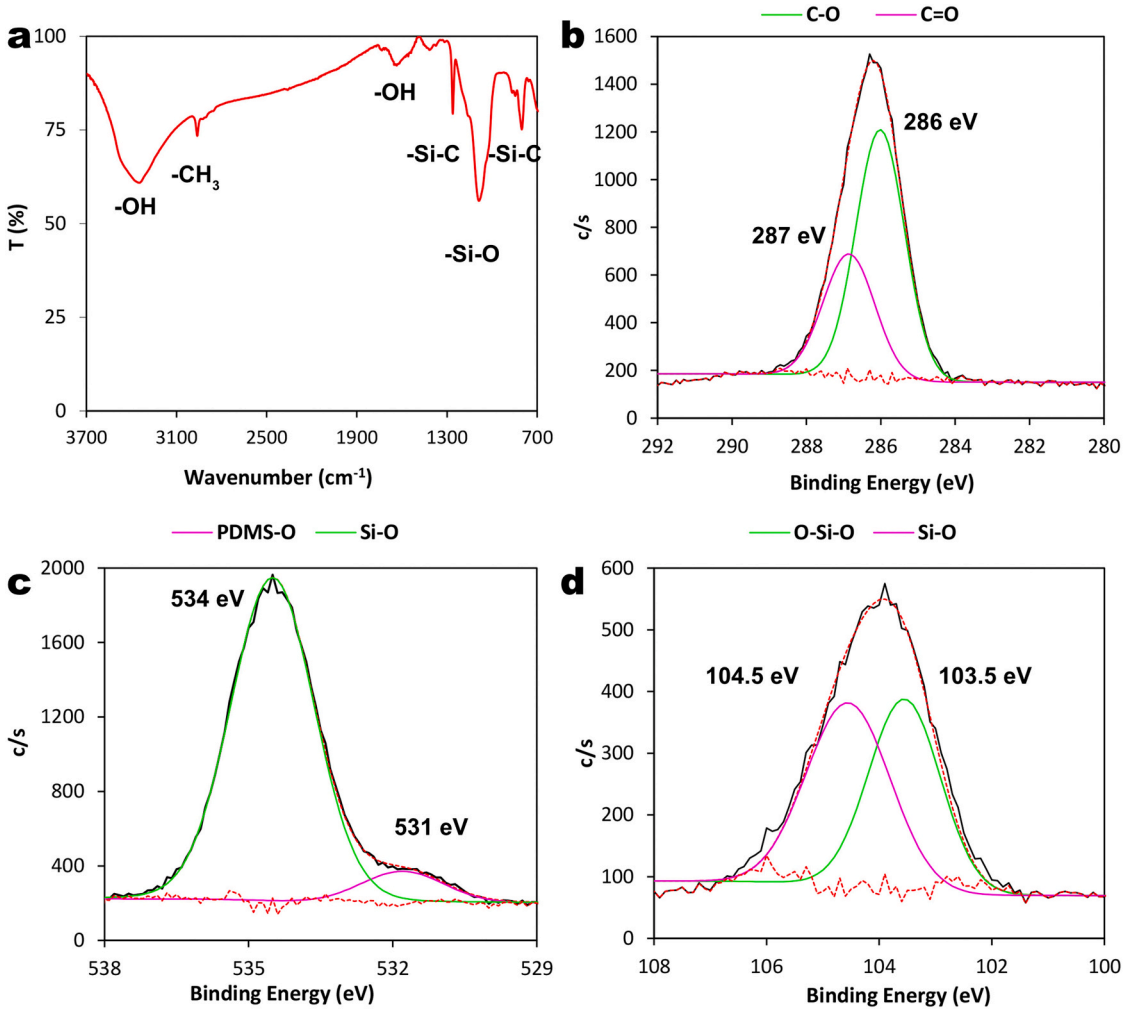

Fig. 3. Surface chemical composition: (a) ATR-FTIR of the superhydrophobic mesh revealing the presence of PDMS and HR-XPS analysis corresponding to (b) C-1s, (c) O-1s and (d) Si-2p.

vSi—C respectively [39]. HR-XPS was used to confirm the presence of the chemical compounds found in the ATR-FTIR characterization. In the C-1s (Fig. 3 b) the signal was deconvoluted into two peaks at 286 eV and 287 eV assigned to C—O and C═O respectively [40,41]. In the case of O-1s (Fig. 3 c) there were two different deconvolutions at 531 eV assigned to PDMS-O [41,42] and 534 eV the from O—Si—O bonds in PDMS [41,43]. Finally, in the case of Si-2p (Fig. 3 d) two deconvolutions were found at 103.55 eV relative to O—Si—O-quartz [41,44,45] and 104.55 eV related to the silicate form (Si—O_4) [41,46].

Overall, the combination of ATR-FTIR as well as the HR-XPS characterization techniques at the surface level led to the identification of the main chemical compound at the surface level that corresponds to the PDMS generation a coating layer throughout the 304 SS mesh. In fact, it is the presence of this compound that causes a decrease in the surface free energy of the coating and, combined with the hierarchical structure as observed in the FESEM micrographs, promotes the superhydrophobic properties.

4.3. Wetting properties

It is well known that the contact angle measurements are a key parameter for defining the wettability properties of a surface. Here, we determined the WCA, SA, CAH as well as the OCA of the PDMS modified 304 SS mesh. Additionally, the WCA and the OCA for the HDPE-MP were also measured. The WCA for the etched 304 SS was 37 ± 2°, showing hydrophilic properties, while after the PDMS modification it was 159 ± 5°, clearly indicating superhydrophobicity (Fig. 4 a) with a SA = 1 ± 1° and a CAH 1 ± 1° and exhibiting self-cleaning properties (Fig. S5). In the case of the superhydrophobic mesh, the OCA = 0 ± 1° showed superoleophilic properties (Fig. 4 b). With regard to the HDPE-MP, the measurements were WCA = 136 ± 2° and for the OCA = 1° with instant absorption, showing hydrophobicity and superoleophilicity respectively (Fig. 4 c and d).

The wetting properties of the water droplet on the PDMS@304SS mesh correspond to a low adhesion state where the cavities from the hierarchical structure were filled with air instead of water what is clearly assigned to the Cassie-Baxter [47], while CAH measurements showed that the surface presents a wetting mode assigned to the lotus leaf effect [48,49]. In contrast, in the presence of hexane, the cavities were filled with the organic solvent instead of air, generating the superoleophilic properties with instant oil sorption. Additionally, the WCA and the OCA measurements of HDPE-MP showed more affinity to hexane than to water because of the intrinsic hydrophobicity of polymeric materials due to their low surface free energy, which in turn is caused by their chemical composition and in particular by the presence of long chains of C—H bonds from the $(CH_2\text{-}CH_2)_n$ polymer [50]. Apart from determining the contact angles it was also interesting to study the durability of the superhydrophobic PDMS@304SS mesh in different aqueous media. At different pH values (pH = 0, 1, 4, 7, 9, 12 and 14) the WCA measurements did not change and were above 150° in the whole range of pH values. This behavior shows that the superhydrophobic mesh was resistant to corrosive media, revealing that pH has no effect on the wetting properties of the surface, and it is because the high chemical stability of PDMS against different solutions because there were non-ionizable functional groups at the coating surface.

One of the most challenging issues of superhydrophobic surfaces is their durability against abrasion. For this reason, the superhydrophobic PDMS@304SS mesh was also studied with an abrasive paper test [51]. As seen in Fig. 5, the surface was slightly affected because some parts of the upper layers of the superhydrophobic surface were removed (Fig. 5 a and b) or were smoother than the surface observed before the abrasion. After observing the damage caused by the abrasive test we wanted to study the chemical composition of the PDSM@304SS and to determine how the test affected the surface. Fig. 5 c shows the ATR-FTIR spectrum of the surface after the abrasion. It can be seen that between 3700 cm^{-1} and 3100 cm^{-1} the band corresponds to vO—H of the oxide layer and ca. 3000 cm^{-1} there is the v_aCH_3, while there is an intense band ca. 1100 cm^{-1} assigned to vSi—O and ca. 1250 cm^{-1} assigned to δSi—C. These bands are characteristic of the PDMS used to coat the surface and indicate that, despite the damage suffered during the abrasion, the PDMS

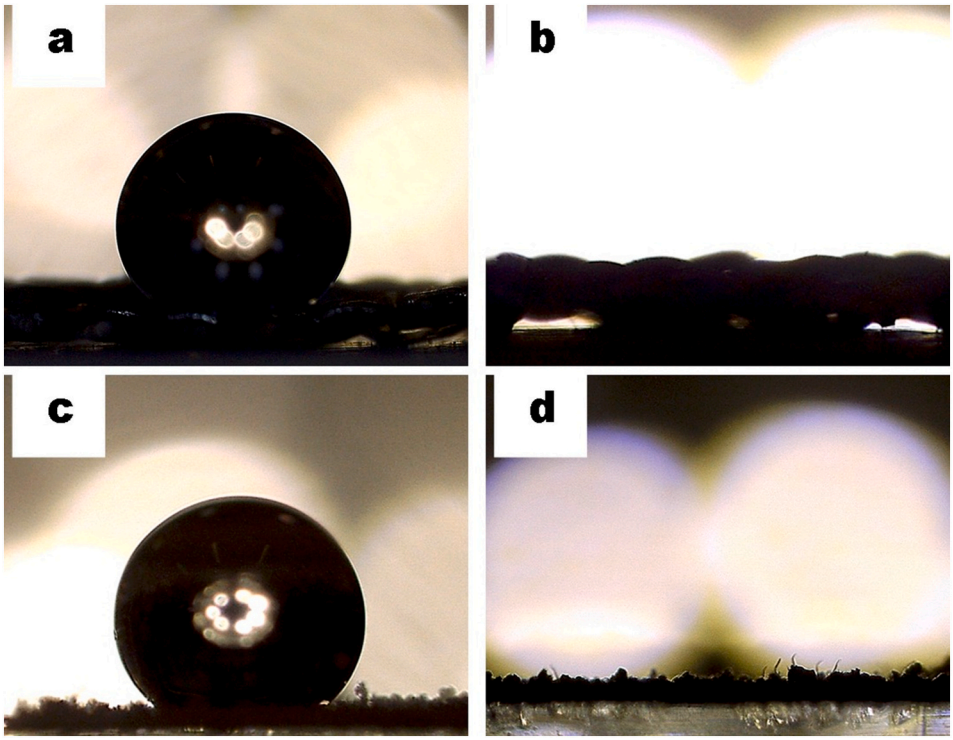

Fig. 4. Contact angle measurements: a) PDMS@304SS mesh with a WCA = 159 ± 5° and b) OCA ~0 ± 1°. For the HDPE-MP particles, c) WCA = 136 ± 2° and d) the OCA = 0 ± 1° with instant and total absorption.

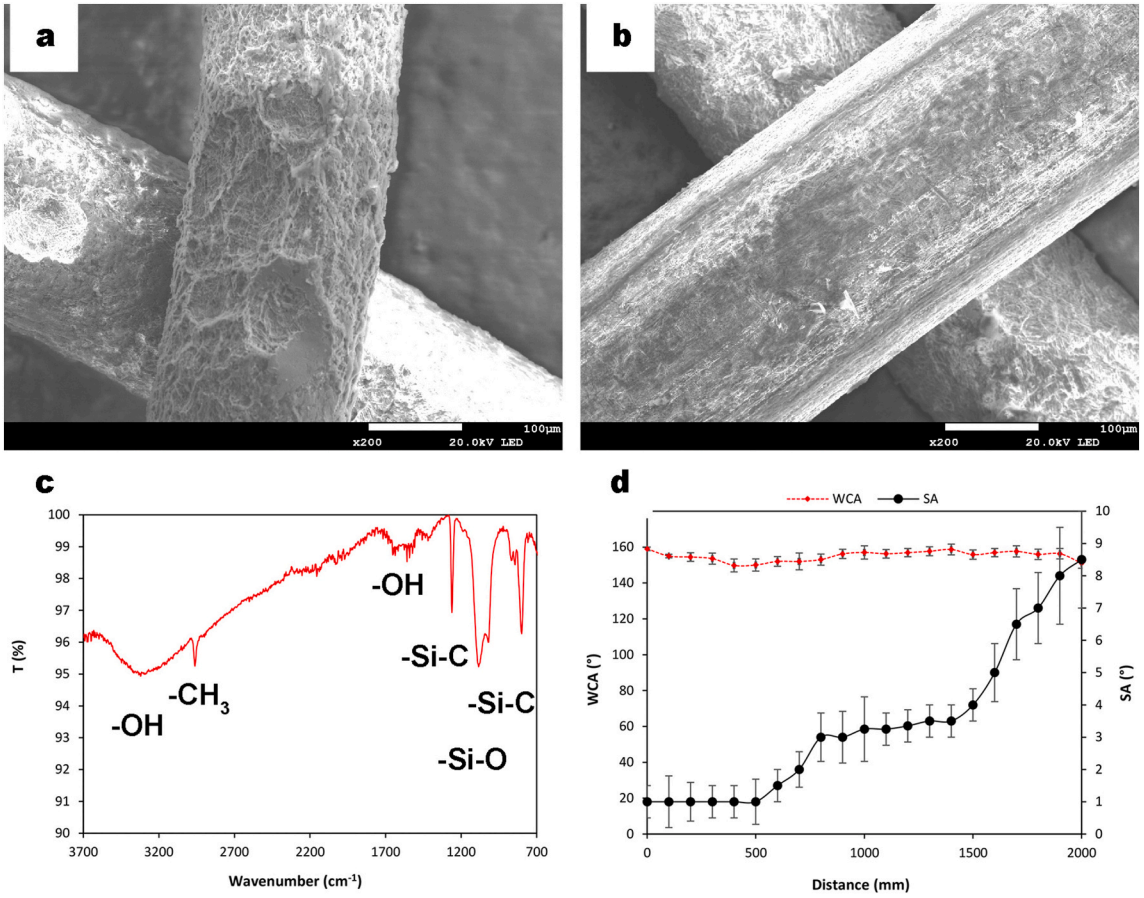

Fig. 5. Durability test of the PDMS@304SS mesh: a and b) FESEM micrograph showing two different parts where the surface was affected by the abrasive paper, c) ATR-FTIR spectra showing that after abrasion the PDMS coating was present and d) evolution of the WCA and SA after 2000 mm.

coating remained adhered to the 304SS mesh and the chemical composition at the surface level remained unaltered. Additionally, the EDS of the surface after the abrasive test presented a slight decrease in the Si peak revealing that a small quantity of PDMS had been removed (Fig. S6). Durability was determined by measuring the WCA and SA during the abrasive paper test (Fig. 5 d). The results showed that the WCA remained constant throughout the experiment while the SA increased from 1 ± 1° to 8.5 ± 1.5°. In fact, in the variation of the SA measurements three different stages could be identified during which the adhesion of water droplets changed. Firstly, the SA remained constant up to 500 mm of the abrasion test, indicating that the surface was clearly coated with PDMS and still presented the necessary hierarchical structure to show high water repellency and low water adhesion. In this case, the surface presented a similar morphology to those previously described after the chemical etching and the PDMS coating. Then, the SA increased from 1 ± 1° to 3.5 ± 1° and remained constant until 1400 mm. In this second stage where the measurements revealed that the water adhesion increased, the upper areas of the PDMS coating were shown to be removed slightly by the abrasive paper but the polymer and the hierarchical structure were still present despite the observation of some larger cavities (Fig. 5 a). After this, the SA rose to 8.5 ± 1.5° until 2000 mm of abrasion. As seen, this final evolution indicates that the PDMS layer as well as the hierarchical structure obtained were clearly damaged (Fig. 5 b) but the surface still presented superhydrophobicity (WCA = 151 ± 1.5°). Additionally, the roughness of the PDMS@304SS mesh after abrasion was compared to the RMS achieved after the surface modification process. In this regard, the RMS decreased from 2.54 ± 0.1 µm to 1.31 ± 0.2 µm after the abrasion, revealing that the surface was affected by the abrasive paper test and was then reasonably smooth. If the RMS results are compared to the WCA and SA, it can be seen that although the hierarchical structure was affected, and because of its homogeneous chemical composition the WCA was also slightly affected, as the roughness decreased the SA increased, indicating that the water adhesion properties after 2000 mm decreased slightly during the abrasive paper test.

Taking into account the durability measurements, it is important to stress that because the PDMS@304SS mesh had a highly homogeneous chemical composition the surface was strongly robust in this abrasive condition [52]. In fact, the reason why the durability was very high is because there were no pinning sites introduced to the hierarchical structure and the cavities of the superhydrophobic coating were still filled with air when it was in contact with water instead of being filled with the liquid phase, which would notably increase its water adhesion and consequently decrease the WCA [53]. In fact, the durability of the coating is directly related to the adherence and abrasion durability of the composite oxide/PDMS layer. If the composite coating is completely removed (or only the PDMS layer) the surface would not present superhydrophobic properties and its WCA would fall dramatically to a hydrophilic state (WCA < 90°).

4.4. Microplastics removal

In order to evaluate further the ability of the superhydrophobic mesh to remove HDPE-MP, a lab-made device was designed, as shown in Fig. 6 a. Here, once the aqueous phase containing microplastics (Fig. 6 b) was put in contact with the organic phase (hexane) in the dropping funnel, the HDPE-MP migrated from water to the water-oil interface under stirring. Then, the two phases were separated and while the water slid

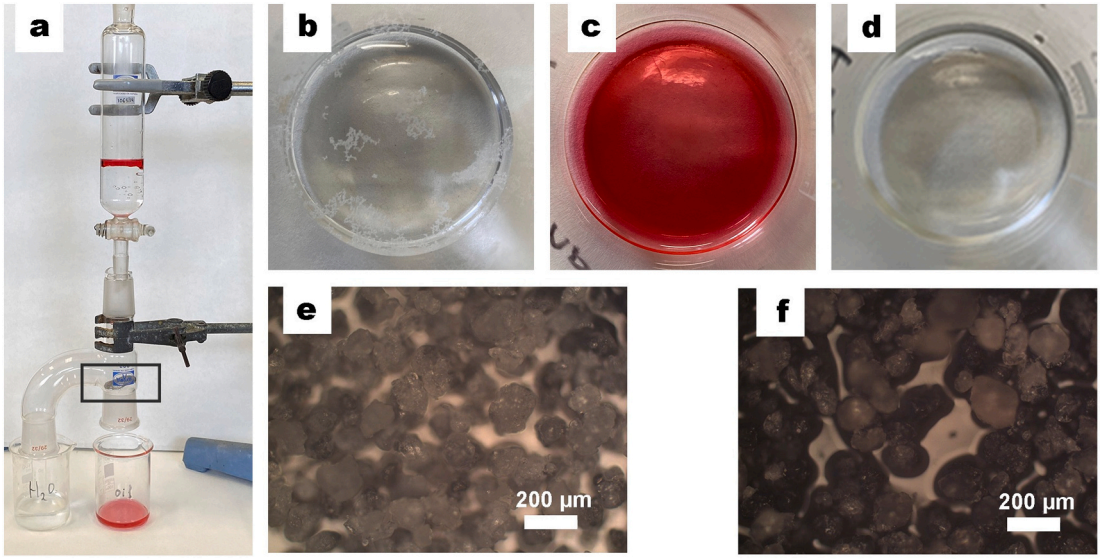

Fig. 6. Separation process of HDPE-MP: a) the lab-made device for MP removal, b) the aqueous phase containing HDPE-MP, c) the oil phase (red) where HDPE-MP were collected, d) pure water collected after the separation. Optical micrographs comparing the MP: e) before and f) after the removal. (For interpretation of the references to color in this figure legend, the reader is referred to the web version of this article.)

through the superhydrophobic mesh because of the SA (1 ± 1°), the organic phase containing the HDPE-MP was collected in the mesh as well as in the beaker (Fig. 6 c) leaving a pure aqueous phase without presence of either oil or HDPE-MP (Fig. 6 d). In fact, while the organic phase was in contact with the PDMS@304SS mesh two mechanisms could be observed: Initially, the hexane containing HDPE-MP completely permeates the surface while the solid pollutants spread through the whole surface, as hexane does. After this, once the mesh was saturated with the organic phase, the oil droplets containing HDPE-MP fell into the beaker driven by gravity force. It should be borne in mind that because of the superoleophilic properties of the PDMS@304SS mesh a small quantity of oil as well as HDPE-MP remained adhered to the surface, but this did not reduce the ability to remove these pollutants as neither the oil nor the HDPE-MP moved to the aqueous phase. Additionally, the HDPE-MP size was not affected by the use of the organic solvent and remained constant at 133 ± 35 μm throughout the separation process (Fig. 6 e–f) showing that the solid pollutants did not break down or swell when hexane was used; this is particularly important because some wastewater treatments operate under high water pressure, and MP often break down into smaller nanoplastics and may be poured back into the natural waters or even consumption water. Furthermore, to evaluate the ability of the superhydrophobic mesh to remove HDPE-MP, the removal efficiency (η) described as Eq. (1) could be used:

$$\eta\ (\%) = m_{MP}/m_{total}\cdot 100 \quad (1)$$

where m_{MP} is the HDPE-MP mass collected in the beaker as well as in the mesh and m_{total} is the total mass of HDPE-MP added in the dropping funnel. The process completely removed the HDPE-MP as well as the organic phase with a η = 99 ± 1 %, removed 2.8 mg HDPE-MP per 1 mL of hexane, and completely removed the organic solvent. Moreover, the removal of MP using the PDMS@304SS and other types of oils can also be carried out, exhibiting high efficiencies for petroleum ether (η = 98 ± 1 %) or xylene (η = 99 ± 2 %). These results show that the superhydrophobic/superoleophilic character of the PDMS@304SS mesh promotes the separation of HDPE-MP into different kinds of oils and that the wetting properties are the main reason for removing the solid pollutants. The flux of the system was also studied at 3.0 mL/s, 1.5 mL/s and 1.0 mL/s. It was found that the difference in pouring flux did not interfere with the efficiency of the pollutant removal and, as seen in case of the highest flux (3 mL/s), the removal efficiency was 99 ± 1 % for 1.5 mL/s and 1.0 mL/s.

In addition to determining this new application of superhydrophobic surfaces and also its efficiency, it is worth noting that the PDMS@304SS mesh and the process itself can be reused up to 20 times without loss of either superhydrophobicity or removal efficiency. During the reusability test, the WCA, the SA and the OCA remained relatively constant near 159 ± 7°, 1 ± 1° and 0 ± 1° respectively. This shows clearly that the superhydrophobic PDMS@304SS coating was not affected or dissolved after 20 rounds of the removal process, underlining the chemical stability of PDMS. As for removal efficiency, it also remained constant (99 ± 1 %) and the whole quantity of HDPE-MP as well as organic solvent used was removed after each step. These results showed that the superhydrophobic PDMS@30SS mesh presents long-term stability and so can be repeatedly reused without losing its wetting properties and maintains high durability against different oils, pH and abrasion.

With regard to the wetting properties of HDPE-MP described above, it is necessary to consider the behavior of these persistent solid pollutants at the interface between water/air and water/oil so as to identify the mechanism driving the separation. As shown, the superhydrophobic PDMS@304SS mesh could be used to remove oil and HDPE-MP from water with extremely high efficiencies. But the reason why these persistent solid pollutants can be easily removed by this method remains to be elucidated. One explanation for the oil/water separation containing HDPE-MP might be obtained by considering the well-known Young–Laplace equation [54,55] (Eq. (2)):

$$\Delta P_{it} = -4\gamma\ (\cos\theta)/d \quad (2)$$

where ΔP_{it} is the intrusion pressure, γ is the oil/water interfacial tension, θ is the contact angle of the liquid (oil or water) with the solid surface (PDMS@304SS mesh), and d the mesh hole size. Considering that γ = 0.25 mN/m for the system hexane/water and the hole diameter was 0.7 mm, it can be deduced that the Laplace pressure is positive for a WCA = 154° and negative for OCA = 0°. This indicates that water cannot pass through the PDMS@304SS mesh, while hexane may permeate the solid completely and pass through the mesh, leading to oil/water separation [56].

The MP themselves can be considered as colloids and so their physicochemical properties such as wetting can be attributed to the coating surface interaction between particles as well as their chemical composition [57,58]. From a surface point of view, the removal could be

explained by considering two different interactions between the PDMS@304SS mesh and the HDPE-MP, namely the interparticle interactions and the binding energy of the HDPE-MP to the solid-liquid interface. On the one hand, the interactions between particles in water are caused by the dissociation of organic functional groups found at the surface of polymers such as hydroxyls or carboxylates which causes a certain negative polarization of the MP surface (—COOH → —COO^-/—OH → —O^-). As this phenomenon is repeated on each particle surface, it increases the repulsion between MP and prevents their aggregation, thus making their removal from water difficult. On the other hand, the binding energy of MP indicates that as the size of the particles decreases, their wetting properties tend to be more hydrophilic because the binding energy decreases, making the removal of the solid pollutants from the water more difficult [59–62]. Taking both these factors into account, it can be deduced that when they are combined in an aqueous phase, the MP tend to be located in water and so it is very difficult to remove them by using surface procedures. In this scenario and from a surface point of view, it is necessary to change the surrounding media of MP in order to remove them from water. When the liquid phase that surrounds the MP is an oil, the functional groups cannot dissociate in the organic media, and so the negative electronic charge present in water is no longer present at the MP surface. Then, in the absence of this repulsion, they can easily aggregate rather than disperse because the binding energy is more favorable in the organic medium than in the aqueous one. Once the HDPE-MP migrate to the oil phase, due to a better affinity with the organic solvent (OCA = 0 ± 1°) than with water (WCA = 136 ± 2°), at the surface of PDMS@304SS mesh, the aqueous phase is replaced by the organic phase and the latter completely fills all the pockets of the hierarchical structure, thus increasing the capillary forces between the MP and the PDMS surface pockets. In the coating surface, there is no dissociation of surface functional groups and so the HDPE-MP cannot be repealed by electrostatic interactions between the pollutants and the coating surface. At this point, as the HDPE-MP are found in the oil phase and because of the superoleophilic properties of the PDMS coating, hydrogen bond interactions between the solid pollutants and the PDMS are also present (Fig. 7). In fact, these interactions are formed repeatedly through the completely coated surface and the HDPE-MP between the hydrogen atom from the HDPE and the oxygen from the PDMS [63].

In general terms, the organic phase plays a key role in the removal of solid pollutants like HDPE-MP by using superhydrophobic surfaces. In fact, the oil phase presents three different advantages over other MP traditional methods: i) it causes the MP to migrate from the aqueous phase to the organic one because of their intrinsic oleophilic properties; ii) it promotes the aggregation of microplastics because there is no surface charge and because the binding energy is more favorable while there are also hydrogen bond interactions between the MP and the surface; iii) the organic phase can be completely removed and containing MP onto the superhydrophobic surface.

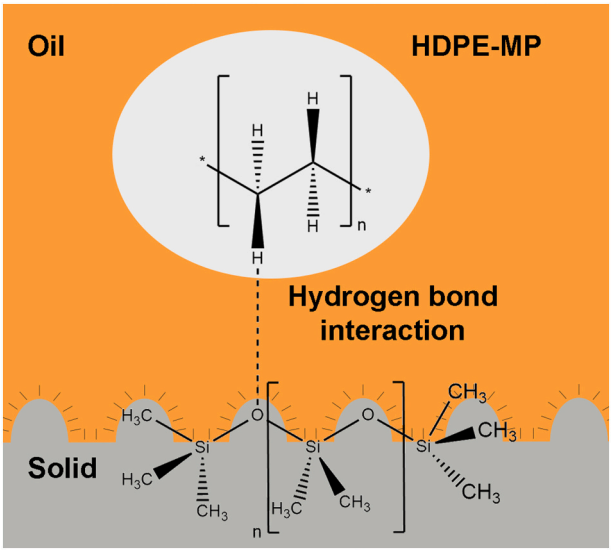

Fig. 7. Hydrogen bond interaction between the PDMS@304SS mesh and HDPE-MP in the oil phase.

Today various methods are available for removing MP from water. They can be divided into conventional and innovative technologies. This classification is not related to their efficiency but to their current use in wastewater treatment plants (WWTP). In fact, as shown in Table 1, conventional techniques (effluents, coagulation, disc filtration or membrane bioreactor) present a wide range of efficiency, from 73 % in case of the use of effluents to 99 % for membrane bioreactor (MBR). Moreover, technologies that are not commonly used in WWTP such as magnetic extraction also present a wide range of efficiency which may limit their application, or entail that they need to be used in combination with other kinds of methods. In fact, membrane-based methods in WWTP are the ones that present the highest removal efficiency of MP, above 99 %, due to their small pore size [4,5]. Despite the extremely high efficiencies of these membranes, they suffer from fouling; this limits their use and means that they have to be changed or treated [64].

The use of a superhydrophobic mesh such as the PDMS@304SS mesh described here achieves complete removal of microplastics by combining the best technologies for this purpose, such as filter technology, and the use of a superhydrophobic surface without fouling and with self-cleaning properties.

5. Conclusions

By combining chemical etching with a $FeCl_3$/HCl/H_2O_2 solution in a 304 stainless steel mesh, followed by PDMS modification, a superhydrophobic (WCA = 159 ± 5°, SA = 1 ± 1° and CAH 1 ± 1°) and superoleophilic (OCA = 0 ± 1°) coating was obtained. Characterization techniques (FESEM, ATR-FTIR and HR-XPS) showed that the 304 stainless steel mesh was completely coated with PDSM as a main compound which reduced the surface free energy of the coating. The durability of the PDMS@304SS mesh was also studied in an abrasion test until 2000 mm as well as at different pH values and in all cases, it shows high durability with few changes in the WCA. This is because the chemical composition of the PDMS@304SS mesh is highly homogeneous.

In addition, the coating was also used to separate oil and HDPE-MP from water with an efficiency of 99 ± 1 %, and removed 2.8 mg of HDPE-MP per 1 mL of hexane. Finally, the reason why the surface could remove microplastics was established: it is due to the migration of the solid pollutants from the aqueous phase to the organic phase because of their intrinsic oleophilic properties and also because of the interparticle

Table 1
Summary of currently available methods for removing MP (PE: polyethylene, PS: polystyrene, PCL: polycaprolactone and PVC: polyvinyl chloride).

Method		Microplastics	Efficiency	Reference
Effluents	H_2O_2/Fe (III)/H_2SO_4	PP and PE	73 %	[65]
Magnetic extraction	Nano-Fe_3O_4	PE, PS, and PP	>80 %	[66]
Coagulation	Al/Fe-based	PE	85 %	[67]
Disc filtration	Polyester mesh (18 μm pore size)	PE, PS and PVC	89.7 %	[68]
Magnetic extraction	HDTMS@Fe	PE and PS	>90 %	[69]
Electrooxidation	Boron-doped diamond anode	PS	89 ± 8 %	[70]
MBR	Biological reactors	PE, PS and PP	99 %	[71]
Superhydrophobicity	PDMS@304SS	HDPE	99 ± 1 %	This work

interactions between the HDPE-MP in the organic phase and with the PDMS coating such the hydrogen bond interaction with the solid pollutants.

CRediT authorship contribution statement

O. Rius-Ayra: Investigation, Conceptualization, Visualization, Methodology, Data curation, Writing - Original draft preparation; A. Biserova-Tahchieva: Investigation, Conceptualization, Visualization, Methodology, Data curation, Writing - Original draft preparation; V. Sansa-López: Investigation, Conceptualization, Visualization, Methodology, Data curation, Writing - Original draft preparation; N. LLorca-Isern: Resources, Supervision, Validation, Writing - Reviewing and Editing.

Funding sources

This research did not receive any specific grant from funding agencies in the public, commercial, or not-for-profit sectors.

Declaration of competing interest

The authors declare that they have no known competing financial interests or personal relationships that could have appeared to influence the work reported in this paper.

Appendix A. Supplementary data

Supplementary data to this article can be found online at https://doi.org/10.1016/j.porgcoat.2022.107009.

References

[1] J.C. Prata, J.P. da Costa, I. Lopes, A.C. Duarte, T. Rocha-Santos, Environmental exposure to microplastics: an overview on possible human health effects, Sci. Total Environ. 702 (2020), 134455, https://doi.org/10.1016/j.scitotenv.2019.134455.
[2] S. Xu, J. Ma, R. Ji, K. Pan, A.-J. Miao, Microplastics in aquatic environments: occurrence, accumulation, and biological effects, Sci. Total Environ. 703 (2020), 134699, https://doi.org/10.1016/j.scitotenv.2019.134699.
[3] Y. Zhang, S. Kang, S. Allen, D. Allen, T. Gao, M. Sillanpää, Atmospheric microplastics: a review on current status and perspectives, Earth-Sci.Rev. 203 (2020), 103118, https://doi.org/10.1016/j.earscirev.2020.103118.
[4] M.R. Karimi Estahbanati, M. Kiendrebeogo, A. Khosravanipour Mostafazadeh, P. Drogui, R.D. Tyagi, Treatment processes for microplastics and nanoplastics in waters: state-of-the-art review, Mar. Pollut. Bull. 168 (2021), 112374, https://doi.org/10.1016/j.marpolbul.2021.112374.
[5] Y. Zhang, H. Jiang, K. Bian, H. Wang, C. Wang, A critical review of control and removal strategies for microplastics from aquatic environments, J. Environ. Chem. Eng. 9 (2021), 105463, https://doi.org/10.1016/j.jece.2021.105463.
[6] S.M. Beladi-Mousavi, S. Hermanová, Y. Ying, J. Plutnar, M. Pumera, A maze in plastic wastes: autonomous motile photocatalytic microrobots against microplastics, ACS Appl. Mater. Interfaces 13 (2021) 25102–25110, https://doi.org/10.1021/acsami.1c04559.
[7] U.B. Gunatilake, R. Morales, L. Basabe-Desmonts, F. Benito-Lopez, Magneto twister: magneto deformation of the water-air interface by a superhydrophobic magnetic nanoparticle layer, Langmuir (2022), https://doi.org/10.1021/acs.langmuir.1c02925 acs.langmuir.1c02925.
[8] G. Peng, M. Xiang, W. Wang, Z. Su, H. Liu, Y. Mao, Y. Chen, P. Zhang, Engineering 3D graphene-like carbon-assembled layered double oxide for efficient microplastic removal in a wide pH range, J. Hazard. Mater. 433 (2022), 128672, https://doi.org/10.1016/j.jhazmat.2022.128672.
[9] B. Bhushan, Y.C. Jung, Natural and biomimetic artificial surfaces for superhydrophobicity, self-cleaning, low adhesion, and drag reduction, Prog. Mater. Sci. 56 (2010) 1–108, https://doi.org/10.1016/j.pmatsci.2010.04.003.
[10] L. Gao, T.J. McCarthy, Contact angle hysteresis explained, Langmuir 22 (2006) 6234–6237, https://doi.org/10.1021/la060254j.
[11] S.M.R. Razavi, J. Oh, S. Sett, L. Feng, X. Yan, M.J. Hoque, A. Liu, R.T. Haasch, M. Masoomi, R. Bagheri, N. Miljkovic, Superhydrophobic surfaces made from naturally derived hydrophobic materials, ACS Sustain. Chem. Eng. 5 (2017) 11362–11370, https://doi.org/10.1021/acssuschemeng.7b02424.
[12] Z. Xu, Y. Zhao, H. Wang, H. Zhou, C. Qin, X. Wang, T. Lin, Fluorine-free superhydrophobic coatings with pH-induced wettability transition for controllable oil-water separation, ACS Appl. Mater. Interfaces 8 (2016) 5661–5667, https://doi.org/10.1021/acsami.5b11720.
[13] C. Schlaich, L. Yu, L. Cuellar Camacho, Q. Wei, R. Haag, Fluorine-free superwetting systems: construction of environmentally friendly superhydrophilic, superhydrophobic, and slippery surfaces on various substrates, Polym. Chem. 7 (2016) 7446–7454, https://doi.org/10.1039/c6py01596d.
[14] M.-C. Bélanger, Y. Marois, Hemocompatibility, biocompatibility, inflammatory and in vivo studies of primary reference materials low-density polyethylene and polydimethylsiloxane: a review, J. Biomed. Mater. Res. 58 (2001) 467–477, https://doi.org/10.1002/jbm.1043.
[15] B.K. Gale, M.A. Eddings, S.O. Sundberg, A. Hatch, J. Kim, T. Ho, Low-cost MEMS technologies, in: Compr. Microsystems, Elsevier, 2008, pp. 341–378, https://doi.org/10.1016/B978-044452190-3.00011-2.
[16] S. Chen, H. Li, X. Lai, S. Zhang, X. Zeng, Superhydrophobic and phosphorus-nitrogen flame-retardant cotton fabric, Prog. Org. Coat. 159 (2021), 106446, https://doi.org/10.1016/j.porgcoat.2021.106446.
[17] S. Zhang, T. Shen, Y. Yang, X. Ma, B. Gao, Y.C. Li, P. Wang, Novel environment-friendly superhydrophobic bio-based polymer derived from liquefied corncob for controlled-released fertilizer, Prog. Org. Coat. 151 (2021), 106018, https://doi.org/10.1016/j.porgcoat.2020.106018.
[18] J. Kim, Y.-J. Lee, J.-W. Park, S.M. Jung, Repeatable separation of microplastics integrating mineral oil extraction and a PDMS-Ni foam adsorbent in real soil, Chem. Eng. J. 429 (2022), 132517, https://doi.org/10.1016/j.cej.2021.132517.
[19] J.-Q. Hu, S.-Z. Yang, L. Guo, X. Xu, T. Yao, F. Xie, Microscopic investigation on the adsorption of lubrication oil on microplastics, J. Mol. Liq. 227 (2017) 351–355, https://doi.org/10.1016/j.molliq.2016.12.043.
[20] C. Sun, Z. Wang, L. Chen, F. Li, Fabrication of robust and compressive chitin and graphene oxide sponges for removal of microplastics with different functional groups, Chem. Eng. J. 393 (2020), 124796, https://doi.org/10.1016/j.cej.2020.124796.
[21] B. Thasma Subramanian, J.P. Alla, J.S. Essomba, N.F. Nishter, Non-fluorinated superhydrophobic spray coatings for oil-water separation applications: an eco-friendly approach, J. Clean. Prod. 256 (2020), 120693, https://doi.org/10.1016/j.jclepro.2020.120693.
[22] R.K. Upadhyay, P.R. Waghmare, Underwater oil drop storage, guided transport, and oil/water separation using surfaces with wettability contrast prepared through a vapor-based etching method, ACS Appl. Mater. Interfaces 12 (2020) 11144–11154, https://doi.org/10.1021/acsami.9b18508.
[23] T. Lü, D. Qi, D. Zhang, K. Fu, Y. Li, H. Zhao, Fabrication of recyclable multi-responsive magnetic nanoparticles for emulsified oil-water separation, J. Clean. Prod. 255 (2020), 120293, https://doi.org/10.1016/j.jclepro.2020.120293.
[24] X. He, T. Wang, J. Huang, J. Chen, J. Li, Fabrication and characterization of superhydrophobic PDMS composite membranes for efficient ethanol recovery via pervaporation, Sep. Purif. Technol. 241 (2020), 116675, https://doi.org/10.1016/j.seppur.2020.116675.
[25] F.S. Kamelian, T. Mohammadi, F. Naeimpoor, Fast, facile and scalable fabrication of novel microporous silicalite-1/PDMS mixed matrix membranes for efficient ethanol separation by pervaporation, Sep. Purif. Technol. 229 (2019), 115820, https://doi.org/10.1016/j.seppur.2019.115820.
[26] B. Wang, S. Peng, Y. Wang, X. Li, K. Zhang, C. Liu, A non-fluorine method for preparing multifunctional robust superhydrophobic coating with applications in photocatalysis, flame retardance, and oil–water separation, New J. Chem. 43 (2019) 7471–7481, https://doi.org/10.1039/C9NJ01318K.
[27] X. Miao, C. Zhu, G. Ren, X. Sun, Y. Li, Rapid, large-scale preparation of non-wetting bismuth oxybromide surface and its practical outdoor applications for the water purification, Appl. Surf. Sci. 515 (2020), 146099, https://doi.org/10.1016/j.apsusc.2020.146099.
[28] U. Baig, A. Matin, M.A. Gondal, S.M. Zubair, Facile fabrication of superhydrophobic, superoleophilic photocatalytic membrane for efficient oil-water separation and removal of hazardous organic pollutants, J. Clean. Prod. 208 (2019) 904–915, https://doi.org/10.1016/j.jclepro.2018.10.079.
[29] S. Rasouli, N. Rezaei, H. Hamedi, S. Zendehboudi, X. Duan, Superhydrophobic and superoleophilic membranes for oil-water separation application: a comprehensive review, Mater. Des. 204 (2021), 109599, https://doi.org/10.1016/j.matdes.2021.109599.
[30] L. Qiu, Y. Sun, Z. Guo, Designing novel superwetting surfaces for high-efficiency oil–water separation: design principles, opportunities, trends and challenges, J. Mater. Chem. A 8 (2020) 16831–16853, https://doi.org/10.1039/D0TA02997A.
[31] M. Zhu, Y. Liu, M. Chen, Z. Xu, L. Li, Y. Zhou, Metal mesh-based special wettability materials for oil-water separation: a review of the recent development, J. Pet. Sci. Eng. 205 (2021), 108889, https://doi.org/10.1016/j.petrol.2021.108889.
[32] B. Jaleh, K. Shariati, M. Khosravi, A. Moradi, S. Ghasemi, S. Azizian, Uniform and stable electrophoretic deposition of graphene oxide on steel mesh: low temperature thermal treatment for switching from superhydrophilicity to superhydrophobicity, Colloids Surf.A Physicochem. Eng. Asp. 577 (2019) 323–332, https://doi.org/10.1016/j.colsurfa.2019.05.085.
[33] Z. Xu, D. Jiang, Z. Wei, J. Chen, J. Jing, Fabrication of superhydrophobic nano-aluminum films on stainless steel meshes by electrophoretic deposition for oil-water separation, Appl. Surf. Sci. 427 (2018) 253–261, https://doi.org/10.1016/j.apsusc.2017.08.189.
[34] J. Wang, J. Xu, G. Chen, Z. Lian, H. Yu, Reversible wettability between underwater superoleophobicity and superhydrophobicity of stainless steel mesh for efficient oil-water separation, ACS Omega 6 (2021) 77–84, https://doi.org/10.1021/acsomega.0c03369.
[35] E.J.Y. Ling, V. Uong, J.-S. Renault-Crispo, A.-M. Kietzig, P. Servio, Reducing ice adhesion on nonsmooth metallic surfaces: wettability and topography effects, ACS Appl. Mater. Interfaces 8 (2016) 8789–8800, https://doi.org/10.1021/acsami.6b00187.

[36] R. Nikosokhan, R. Norouzbeigi, E. Velayi, Preparation of Co3O4 self-cleaning nanocoatings: investigation of ZnO seeded steel meshes, Surf.Interfaces. 23 (2021), 100912, https://doi.org/10.1016/j.surfin.2020.100912.
[37] D. Nanda, A. Sahoo, A. Kumar, B. Bhushan, Facile approach to develop durable and reusable superhydrophobic/superoleophilic coatings for steel mesh surfaces, J. Colloid Interface Sci. 535 (2019) 50–57, https://doi.org/10.1016/j.jcis.2018.09.088.
[38] S. Gao, X. Dong, J. Huang, J. Dong, Y. Cheng, Z. Chen, Y. Lai, Co-solvent induced self-roughness superhydrophobic coatings with self-healing property for versatile oil-water separation, Appl. Surf. Sci. 459 (2018) 512–519, https://doi.org/10.1016/j.apsusc.2018.08.041.
[39] S. Gao, X. Dong, J. Huang, S. Li, Y. Li, Z. Chen, Y. Lai, Rational construction of highly transparent superhydrophobic coatings based on a non-particle, fluorine-free and water-rich system for versatile oil-water separation, Chem. Eng. J. 333 (2018) 621–629, https://doi.org/10.1016/j.cej.2017.10.006.
[40] C. Cao, M. Ge, J. Huang, S. Li, S. Deng, S. Zhang, Z. Chen, K. Zhang, S.S. Al-Deyab, Y. Lai, Robust fluorine-free superhydrophobic PDMS–ormosil@fabrics for highly effective self-cleaning and efficient oil–water separation, J. Mater. Chem. A 4 (2016) 12179–12187, https://doi.org/10.1039/C6TA04420D.
[41] I. Milošev, Ž. Jovanović, J.B. Bajat, R. Jančić-Heinemann, V.B. Mišković-Stanković, Surface analysis and electrochemical behavior of aluminum pretreated by vinyltriethoxysilane films in mild NaCl solution, J. Electrochem. Soc. 159 (2012) C303–C311, https://doi.org/10.1149/2.042207jes.
[42] B. Cha, T. Woo, S. Han, S. Saqlain, H. Seo, H. Cho, J. Kim, Y. Kim, Surface modification of TiO2 for obtaining high resistance against poisoning during photocatalytic decomposition of toluene, Catalysts 8 (2018) 500, https://doi.org/10.3390/catal8110500.
[43] B.J. Cha, T.G. Woo, E.J. Park, I.H. Kim, J.E. An, H.O. Seo, Y.D. Kim, Photo-catalytic activity of hydrophilic-modified TiO 2 for the decomposition of methylene blue and phenol, Curr. Appl. Phys. 17 (2017) 1557–1563, https://doi.org/10.1016/j.cap.2017.07.002.
[44] C. Salazar-Hernández, M. Salazar-Hernández, R. Carrera-Cerritos, J.M. Mendoza-Miranda, E. Elorza-Rodríguez, R. Miranda-Avilés, C.D. Mocada-Sánchez, Anticorrosive properties of PDMS-silica coatings: effect of methyl, phenyl and amino groups, Prog. Org. Coat. 136 (2019), 105220, https://doi.org/10.1016/j.porgcoat.2019.105220.
[45] R. Alfonsetti, L. Lozzi, M. Passacantando, P. Picozzi, S. Santucci, XPS studies on SiOx thin films, Appl. Surf. Sci. 70–71 (1993) 222–225, https://doi.org/10.1016/0169-4332(93)90431-A.
[46] R. Dahiya, G. Gottardi, N. Laidani, PDMS residues-free micro/macrostructures on flexible substrates, Microelectron. Eng. 136 (2015) 57–62, https://doi.org/10.1016/j.mee.2015.04.037.
[47] A.B.D. Cassie, S. Baxter, Wettability of porous surfaces, Trans. Faraday Soc. 40 (1944) 546, https://doi.org/10.1039/tf9444000546.
[48] L. Feng, Y. Zhang, J. Xi, Y. Zhu, N. Wang, F. Xia, L. Jiang, Petal effect: a superhydrophobic state with high adhesive force, Langmuir 24 (2008) 4114–4119, https://doi.org/10.1021/la703821h.
[49] S. Wang, L. Jiang, Definition of superhydrophobic states, Adv. Mater. 19 (2007) 3423–3424, https://doi.org/10.1002/adma.200700934.
[50] M. Alonso Frank, C. Meltzer, B. Braunschweig, W. Peukert, A.R. Boccaccini, S. Virtanen, Functionalization of steel surfaces with organic acids: influence on wetting and corrosion behavior, Appl. Surf. Sci. 404 (2017) 326–333, https://doi.org/10.1016/j.apsusc.2017.01.199.
[51] X. Tian, T. Verho, R.H.A. Ras, Moving superhydrophobic surfaces toward real-world applications, Science 352 (2016) 142–143, https://doi.org/10.1126/science.aaf2073.
[52] T. Verho, C. Bower, P. Andrew, S. Franssila, O. Ikkala, R.H.A. Ras, Mechanically durable superhydrophobic surfaces, Adv. Mater. 23 (2011) 673–678, https://doi.org/10.1002/adma.201003129.
[53] V. Mortazavi, M.M. Khonsari, On the degradation of superhydrophobic surfaces: a review, Wear 372–373 (2017) 145–157, https://doi.org/10.1016/j.wear.2016.11.009.
[54] D. Tian, X. Zhang, Y. Tian, Y. Wu, X. Wang, J. Zhai, L. Jiang, Photo-induced water-oil separation based on switchable superhydrophobicity- superhydrophilicity and underwater superoleophobicity of the aligned ZnO nanorod array-coated mesh films, J. Mater. Chem. 22 (2012) 19652–19657, https://doi.org/10.1039/c2jm34056a.
[55] J. Li, D. Li, Y. Yang, J. Li, F. Zha, Z. Lei, A prewetting induced underwater superoleophobic or underoil (super) hydrophobic waste potato residue-coated mesh for selective efficient oil/water separation, Green Chem. 18 (2016) 541–549, https://doi.org/10.1039/c5gc01818h.
[56] Y. Guan, F. Cheng, Z. Pan, Superwetting polymeric three dimensional (3D) porous materials for oil/water separation: a review, Polymers (Basel) 11 (2019) 1–34, https://doi.org/10.3390/polym11050806.
[57] A. Al Harraq, B. Bharti, Microplastics through the lens of colloid science, ACS Environ. Au. (2021), https://doi.org/10.1021/acsenvironau.1c00016 acsenvironau.1c00016.
[58] W. Zhao, P. Zhao, Y. Tian, C. Shen, Z. Li, P. Peng, C. Jin, Investigation for synergies of ionic strength and flow velocity on colloidal-sized microplastic transport and deposition in porous media using the colloidal–AFM probe, Langmuir 36 (2020) 6292–6303, https://doi.org/10.1021/acs.langmuir.0c00116.
[59] B.P. Binks, Particles as surfactants—similarities and differences, Curr. Opin. Colloid Interface Sci. 7 (2002) 21–41, https://doi.org/10.1016/S1359-0294(02)00008-0.
[60] N. Bizmark, M.A. Ioannidis, D.E. Henneke, Irreversible adsorption-driven assembly of nanoparticles at fluid interfaces revealed by a dynamic surface tension probe, Langmuir 30 (2014) 710–717, https://doi.org/10.1021/la404357j.
[61] B.P. Binks, S.O. Lumsdon, Influence of particle wettability on the type and stability of surfactant-free emulsions, Langmuir 16 (2000) 8622–8631, https://doi.org/10.1021/la000189s.
[62] P. Pieranski, Two-dimensional interfacial colloidal crystals, Phys. Rev. Lett. 45 (1980) 569–572, https://doi.org/10.1103/PhysRevLett.45.569.
[63] X. Rong, X. Chen, P. Li, C. Zhao, S. Peng, H. Ma, H. Qu, Mechanically durable anti-bacteria non-fluorinated superhydrophobic sponge for highly efficient and fast microplastic and oil removal, Chemosphere 299 (2022), 134493, https://doi.org/10.1016/j.chemosphere.2022.134493.
[64] M. Golgoli, M. Khiadani, A. Shafieian, T.K. Sen, Y. Hartanto, M.L. Johns, M. Zargar, Microplastics fouling and interaction with polymeric membranes: a review, Chemosphere 283 (2021), 131185, https://doi.org/10.1016/j.chemosphere.2021.131185.
[65] S. Gündoğdu, C. Çevik, E. Güzel, S. Kilercioğlu, Microplastics in municipal wastewater treatment plants in Turkey: a comparison of the influent and secondary effluent concentrations, Environ. Monit. Assess. 190 (2018) 626, https://doi.org/10.1007/s10661-018-7010-y.
[66] X. Shi, X. Zhang, W. Gao, Y. Zhang, D. He, Removal of microplastics from water by magnetic nano-Fe3O4, Sci. Total Environ. 802 (2022), 149838, https://doi.org/10.1016/j.scitotenv.2021.149838.
[67] B. Ma, W. Xue, C. Hu, H. Liu, J. Qu, L. Li, Characteristics of microplastic removal via coagulation and ultrafiltration during drinking water treatment, Chem. Eng. J. 359 (2019) 159–167, https://doi.org/10.1016/j.cej.2018.11.155.
[68] M. Simon, A. Vianello, J. Vollertsen, Removal of >10 μm microplastic particles from treated wastewater by a disc filter, Water. 11 (2019) 1935, https://doi.org/10.3390/w11091935.
[69] J. Grbic, B. Nguyen, E. Guo, J.B. You, D. Sinton, C.M. Rochman, Magnetic extraction of microplastics from environmental samples, Environ. Sci. Technol. Lett. 6 (2019) 68–72, https://doi.org/10.1021/acs.estlett.8b00671.
[70] M. Kiendrebeogo, M.R. Karimi Estahbanati, A. Khosravanipour Mostafazadeh, P. Drogui, R.D. Tyagi, Treatment of microplastics in water by anodic oxidation: a case study for polystyrene, Environ. Pollut. 269 (2021), 116168, https://doi.org/10.1016/j.envpol.2020.116168.
[71] J. Talvitie, A. Mikola, A. Koistinen, O. Setälä, Solutions to microplastic pollution – removal of microplastics from wastewater effluent with advanced wastewater treatment technologies, Water Res. 123 (2017) 401–407, https://doi.org/10.1016/j.watres.2017.07.005.